

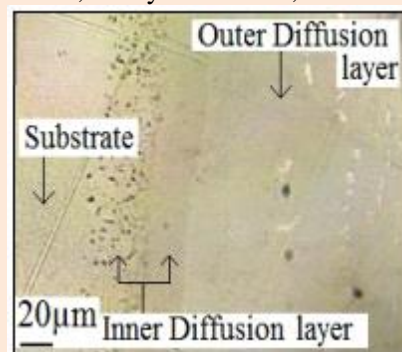
## Research Article

## Hot Dip Aluminizing and Heat Treatment of RAFMS

K. Singh<sup>1</sup>, Shweta Gite<sup>2\*</sup>, Ashlesha B.<sup>2</sup>, K. Bavya Devi<sup>3</sup><sup>1</sup>Fusion Reactor Materials Section, Bhabha Atomic Research Centre, Trombay, Mumbai-400085 India<sup>2</sup>Metallurgical and Materials Engineering, Visvesvaraya National Institute of Technology, Nagpur, India<sup>3</sup>Department of Metallurgical and Materials Engineering, Indian Institute of Technology, Khargapur, India**Abstract**

Reduced Activation Ferritic Martensitic Steel (RAFMS) is a structural material for Test Blanket Module (TBM) in International Thermonuclear Experimental Reactor (ITER). Coating is necessary to improve performance of RAFMS. RAFMS was coated by hot dipping in the molten bath containing Al-2.25 wt.% Si. Heat treatment was performed at 750 °C for 5, 10, 15, 25, 50, and 75 h. Thickness of the inner diffusion layer increased with increase in the duration of heat treatment. Hardness of the outer layer was more than the inner layer. Outer layer consists of primarily Fe<sub>2</sub>Al<sub>5</sub> phase, intermediate zone FeAl phase and the porous band a mixture of FeAl, Fe<sub>3</sub>Al and α-Fe(Al) phases. Scratch test showed that the sample heat treated for 75 h exhibited better performance relatively.

**Keywords:** Aluminizing, heat-treatment, microhardness, X-ray diffraction, Scratch test.

**\*Correspondence**

Author: Shweta Gite

Emails: shwetagite889@gmail.com

**Introduction**

India is one of the participating countries to develop the test blanket module (TBM) for International Thermonuclear Experimental Reactor (ITER). India is developing the lead–lithium cooled ceramic breeder (LLCB) as the blanket concept [1, 2]. It consists of lead–lithium eutectic, which acts as multiplier and coolant with Lithium titanate as the ceramic breeder material. In the case of liquid metal coolant in magnetic confinement, flow of the melt in the strong magnetic field causes a high Magneto-hydrodynamic (MHD) drag. Therefore, coatings are mandatory to improve the performance of the material used in the TBM. Reduced Activation Ferritic Martensitic Steel (RAFMS) is proposed as the structural material for the TBM. The main purposes of forming the coating on RAFMS are to produce a tritium permeation barrier [3-6], improve the corrosion resistance against liquid metals at high temperatures [7], provide helium containment in helium-cooled structures [8] and provide electrical insulation for mitigating magneto hydrodynamic (MHD) effects in self-cooled liquid metal (Pb-Li) systems [9-13].

The desired characteristics of the coatings are high thermal conductivity, good irradiation resistance, mechanical integrity with the substrate material, and uniform coating formation in complex geometries. Development of aluminide layer on RAFMS is one such potential option. To achieve this hot dip aluminizing (HDA) combined with post heat treatment is being explored [14]. Earlier studies showed that hot-dip aluminized and subsequently heat treated steel seem to offer a good possibility to produce aluminide coating with improved properties [14-17]. Heat treatment performed on 9Cr–1Mo Grade 91 steel samples at different temperatures for specific duration showed that the adhesion of the coating in case of samples heat treated at 950 °C was better as compared to the samples heat treated at 650/750 °C [17]. A study showed that heat treatment with superimposed pressure has significant influence on the structure of HDA steel sheets; high pressure suppresses the formation of porous bands by compressing the pores during formation [15]. In the present investigation, hot dip aluminizing was carried out on RAFMS samples in aluminium (Al) melt containing small amount of silicon (Si). Addition of small amounts of Si to the Al melt helps reduce the thickness of brittle intermetallic layer and also the growth of the intermetallic layer occurs slowly [18, 19]. Post dipping, samples were heat treated at 750 °C for various durations. Temperature for heat treatment was selected

at 750 °C because austenitisation of RAFMS begins above 800 °C [20]. The aluminized and heat treated samples have been characterized by various techniques.

## Experimental

RAFMS was used as the substrate material. RAFMS was analyzed for chemical composition by X-ray fluorescence (XRF) technique. Composition of RAFMS was Cr-9.04, W-1.40, Mn-0.56, Ta-0.06, V-0.24 and Fe-88.40 wt.%. Rectangular specimens of the dimension 15 mm by 10 mm having 2 mm thickness were prepared. On one side of the specimens, a 3 mm hole was made to facilitate hanging by stainless steel (SS) wire for dipping in the melt. Samples were polished with different grit of sandpapers to a surface finish of 0.08 $\mu$ m. Samples were cleaned ultrasonically in an alkaline solution and then rinsed in water. After alkaline degreasing, specimens were pickled in 15% HCl to eliminate any surface oxides that might develop during cleaning procedure and then rinsed in water. To ensure a clean metal surface contact with the melt, fluxing was carried out on the specimens. For fluxing, specimens were immersed in the aqueous flux solution containing 50% NaCl, 40% KCl and 10% Na<sub>3</sub>AlF<sub>6</sub> and dried. For aluminizing, Al-2.25 wt.% Si was used. The alloy was kept in an alumina crucible in a top loading furnace. The furnace was heated to 750 °C. The specimens were dipped manually by wire in the molten bath at 750 °C for 1 min. The aluminized samples were then heat treated at 750 °C for different duration as depicted in **Table 1**. The samples were then air cooled.

**Table 1** Duration of heat treatment (750 °C) for aluminized RAFM steel

Sample	Duration (h)
A	5
B	10
C	15
D	25
E	50
F	75

Aluminized and heat treated samples were cut, mounted and cross sections were polished and seen in the optical microscope. The morphology and compositional analysis of the aluminized and heat treated samples was performed using scanning electron microscopy (SEM - make AIS 2100 Seron Tech) at 20kV coupled with energy dispersive X-ray (EDX) analysis (INCA E350). Line scan and point scan was performed across the cross-section of the coated samples by EDX. Hardness was determined using Vickers micro hardness tester (Future-Tech FM-7 Model) at a load of 50 gf with a dwell time of 5 sec. 3-4 readings were performed at each location and the average values have been reported. X-ray diffraction (XRD) analysis was carried out on the surface of the aluminized and heat treated samples to reveal the phases present. XRD (make Diano) was carried out at 20 mA and 35 kV using CuK $\alpha$  radiations in routine Bragg-Brentano  $\theta$ - $2\theta$  geometry. Scratch tester (CSEM, Revetest) was used to evaluate the adhesion of the coatings. The scratch was carried out on the cross-section at the interface. Constant loads of 3 N and 5 N were applied. The scratch indenter used was a Rockwell type diamond indenter having 200  $\mu$ m tip radius. Friction force, depth of penetration and acoustic emission (AE) signals were recorded online along with the applied load during scratch tests. The scratch tracks were visualized in the optical microscopy immediately after the tests and pictures were taken at the interface.

## Results and Discussion

### Optical microscopy

**Figure 1** shows optical micrographs of aluminized and heat treated RAFMS samples. All the samples showed a wide outer diffusion layer and a thin inner diffusion layer. The outer diffusion layer for samples A and B was about 300-350  $\mu$ m thick and for samples C, D, E, and F it was about 350-400  $\mu$ m. The inner diffusion layer actually consisted of two sub-zones; an intermediate zone towards the outer diffusion layer and a porous band towards the substrate. The formation of pores is due to the difference between the diffusion rates of the interacting metal atoms, termed as the Kirkendall effect [21]. Sample A had the intermediate zone of about 6-8  $\mu$ m thickness and a porous band of 8-10  $\mu$ m thickness (Figure 1a). Sample B showed intermediate zone of 9-11  $\mu$ m thickness and a porous band of 11-13  $\mu$ m

thickness (Figure 1b). Sample C showed intermediate zone of 10-12  $\mu\text{m}$  thickness and a porous band of 12-14  $\mu\text{m}$  thickness (Figure 1c). Sample D showed the intermediate zone of 13-15  $\mu\text{m}$  thickness and a porous band of 18-20  $\mu\text{m}$  thickness (Figure 1d). Sample E showed the intermediate zone of 23-25  $\mu\text{m}$  thickness and a porous band of 28-30  $\mu\text{m}$  thickness (Figure 1e). Sample F showed the intermediate zone of 28-30  $\mu\text{m}$  thickness and a porous band of 33-35  $\mu\text{m}$  thickness (Figure 1f). Thus, it was observed from Figure 1 that the thickness of the intermediate diffusion zone and the porous band increased with increase in the duration of heat treatment, whereas the thickness of the outer diffusion layer did not show much variation. Glasbrenner and Wedemeyer [22] reported a 2 zone structure with an intermediate porous band on aluminizing F82H-mod steel at 700  $^{\circ}\text{C}$  and performing heat treatment at 1040  $^{\circ}\text{C}/0.5$  h, 750  $^{\circ}\text{C}/1$  h. Bouché et al. [23] reported the formation of two intermetallic layers, namely,  $\text{Fe}_2\text{Al}_5$  and  $\text{FeAl}_3$ , when solid iron is dipped in liquid Al over the temperature range of 700  $^{\circ}\text{C}$  to 900  $^{\circ}\text{C}$ . They reported that the growth behaviour is initially non parabolic which is followed by parabolic. Fu-cheng et al. [24] observed that the tongue-like morphology of the  $\text{Fe}_2\text{Al}_5$  layer becomes less distinct and disappeared on aluminizing at 800  $^{\circ}\text{C}$  for Si content above 1 wt.%. They also observed that the growth rates of the  $\text{Fe}_2\text{Al}_5$  and  $\text{FeAl}_3$  layers decreased with increasing Si content in the molten bath and optimum result were obtained at 2-3 wt. % Si.

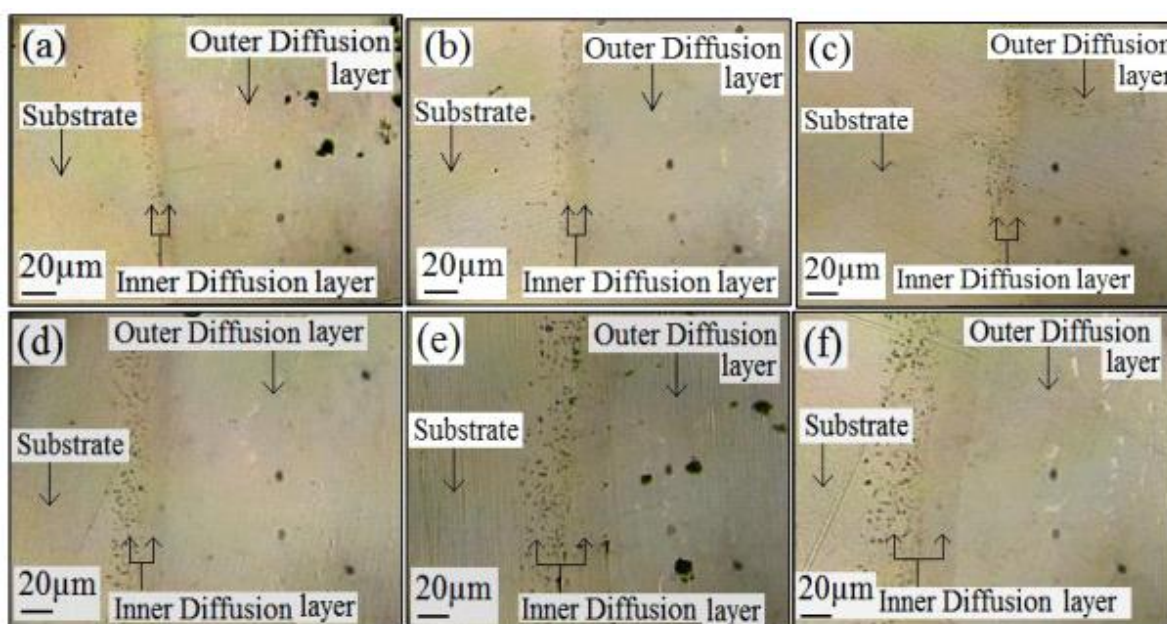


**Figure 1** Optical images of the cross-sections of RAFM steel aluminized and heat-treated (a) sample A; (b) sample B; (c) sample C; (d) sample D; (e) sample E; and (f) sample F

**Figure 2** shows the plot between the thickness of inner layers (i.e. intermediate zone and porous band) and duration of heat treatment. The thickness of porous band is more than that of the intermediate zone at any specific duration of heat treatment. Polynomial fit with an order of 2 was observed to be best fit for the increase in the thickness of inner layers with duration of heat treatment. The equations for variation in thickness of intermediate zone and porous band with heat treatment time are shown in the graph.

### Microhardness

Microhardness for all the samples were taken across the cross-section of aluminized and heat treated samples. Microhardness for samples A, B, C and D varied between 850-950 HV across the outer diffusion layer, whereas for samples E and F it varied between 750-850 HV. Sample A showed micro hardness of about 640 HV in the intermediate band and 340 HV in the porous band. Sample B showed micro hardness of about 580 HV in the intermediate band and 332 HV in the porous band. Sample C showed micro hardness of about 542 HV in the intermediate band and 315 HV in the porous band. Inner diffusion layer for sample D showed micro hardness of about 455 HV in the intermediate band and 338 HV in the porous band. Inner diffusion layer for sample E showed micro hardness of about 386 HV in the intermediate band and 312 HV in the porous band. Inner diffusion layer for sample F showed micro hardness of about

404 HV in the intermediate band and 332 HV in the porous band. **Figure 3** depicts the micro-hardness of samples C, D, E and F for simplicity. Thus, it was observed that the hardness of the outer diffusion layer decreased with increase in the duration of heat treatment. Simultaneously, hardness of the intermediate diffusion zone also decreased with increase in the duration of heat treatment till 50 h but it increased when heat treatment was performed for a period of 75 h. Hardness of the porous band varied in a short range with heat treatment duration. Variation in hardness was due to the change in Fe:Al (as observed in EDX analysis) with the increase in duration of heat treatment. As reported by Li et al. [25], the hardness of the outer diffusion layer (750-950 HV) is in good agreement with micro hardness values for the brittle  $\text{Fe}_2\text{Al}_5$  and  $\text{FeAl}_3$  phases, for mild steel hot dip aluminized with 3 wt.%Si (780 °C, 10 min) and diffusion annealed (640 °C, 30 min). They observed that the hardness of inner diffusion layer was low due to the presence of Fe rich  $\text{Fe}_3\text{Al}$  and  $\alpha\text{-Fe(Al)}$  phases. They also noted that  $\text{Fe}_3\text{Al}$  phase had good toughness and lower hardness value as compared to Al rich phases  $\text{Fe}_2\text{Al}_5$  and  $\text{FeAl}_3$ .

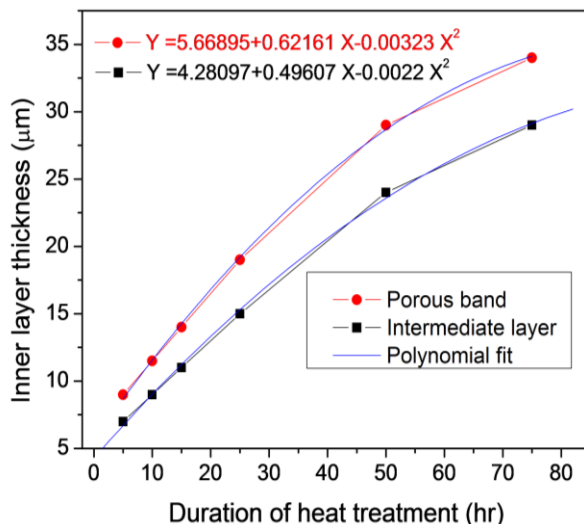


**Figure 2** Thickness variation of inner zones with heat treatment duration (T=750 °C)

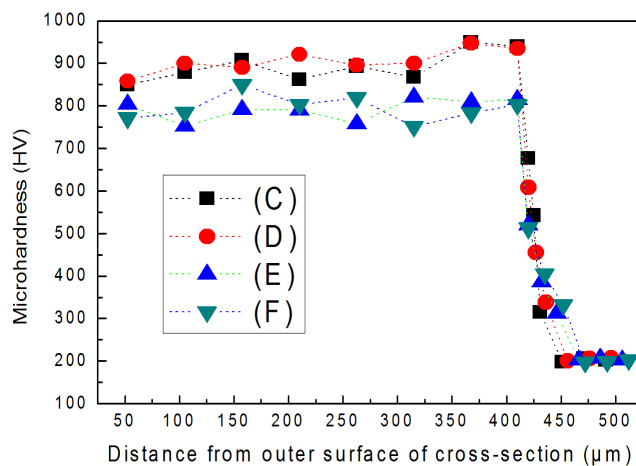


**Figure 3** Microhardness on the cross-section of samples C, D, E and F

### SEM and EDX analysis

SEM and EDX analysis (point scan and line scan) of all the aluminized and heat treated samples was performed. EDX analysis was performed at various locations across the cross section of the samples. However results for only representative samples are shown. **Figure 4** shows the SEM images for samples C and F showing the distinct outer diffusion layer, intermediate zone and porous band. EDX point scan analysis was performed at 4 spots (spectra) across the cross-section of all the coated and heat treated samples as shown in Figure 4. Spectra 1, 2, 3 and 4

correspond to substrate, porous band, intermediate zone and outer diffusion layer respectively. EDX point and line scan analysis was repeated at few places to observe variation in the composition in the same zone. However variation observed was too less to be discussed. **Figure 5** shows the EDX point scan analysis of spectrum 3 for samples C and F. Fe:Al ratio in the outer diffusion layer of samples C, D, E and F was  $\sim 1:2.5$  which corresponds to primarily  $\text{Fe}_2\text{Al}_5$  phase, however in the intermediate zone adjacent to the outer diffusion layer the ratio changes to  $\sim 1:1$  which corresponds to primarily FeAl phase. Fe:Al ratio in the porous band was varying from 1:0.43 to 1:0.9 which may correspond to a mixture of FeAl,  $\text{Fe}_3\text{Al}$ , and  $\alpha\text{-Fe(Al)}$  phases [25]. Al content in the porous band decreased with increase in the duration of heat treatment. Fe:Al ratio in the porous band was 1:0.9 for sample C, 1:0.52 for sample E, and 1:0.43 for sample F. This resulted in increase in the Fe rich compounds formed with the increase in duration of heat treatment. Formation of Fe rich compounds is desirable due to their high toughness value [25]. Serra et al. [26] reported formation of  $\text{Fe}_2\text{Al}_5$ , FeAl<sub>2</sub> and FeAl phases in outer, intermediate and inner layers respectively on performing heat treatment in air at 1023 K (for 15 and 30 h) on hot dip aluminized MANET II steel. Li et al. [27] observed the presence of similar phases like  $\text{Fe}_2\text{Al}_5$ , FeAl,  $\text{Fe}_3\text{Al}$ , and  $\alpha\text{-Fe(Al)}$  phases in the aluminized and diffusion annealed steel.

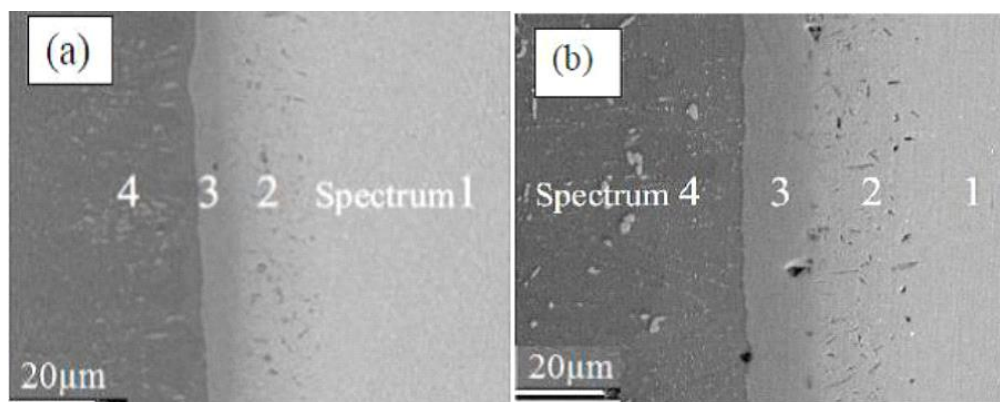


**Figure 4** SEM of cross-section of (a) sample C; and (b) sample F

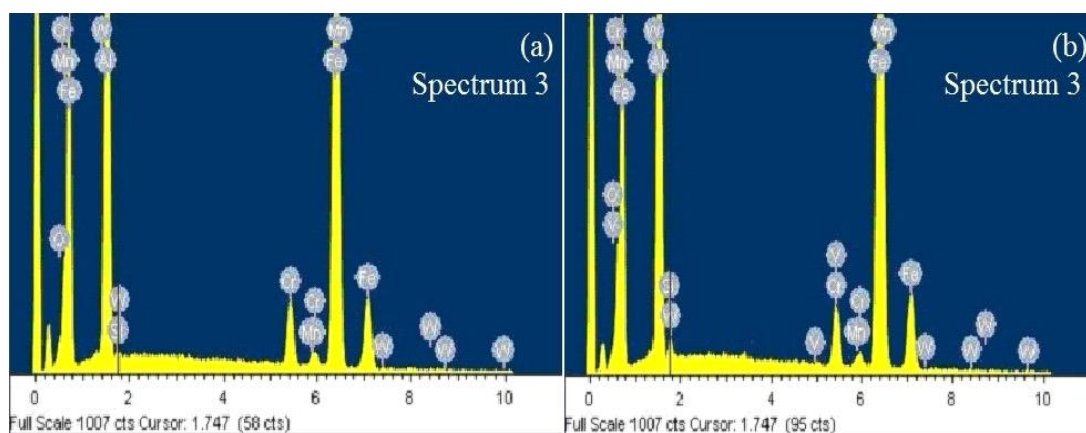


**Figure 5** EDX spot analysis at spectrum 3 on the cross-section of (a) sample C; and (b) sample F

**Figure 6** depicts line scan analysis for sample F. The variation of different elements can be clearly seen from the plot. The outer diffusion layer shows prominent concentration of Al. As we move towards the substrate, Al content decreases and Fe and Cr contents increase. Intermediate zone shows nearly equal amounts of Fe and Al (with Fe:Al varying from 1: 1.2-0.9). Porous band consists of more amount of Fe than Al indicating presence of Fe-rich phases.

### X-ray Diffraction

X-ray diffraction was carried out on the slightly polished surface of aluminized and heat treated samples to reveal the phases present in the outer diffusion layer.  $\text{Fe}_2\text{Al}_5$  phase was found to be present in the outer diffusion layer. A representative analysis is depicted in **Figure 7** for samples A and D.

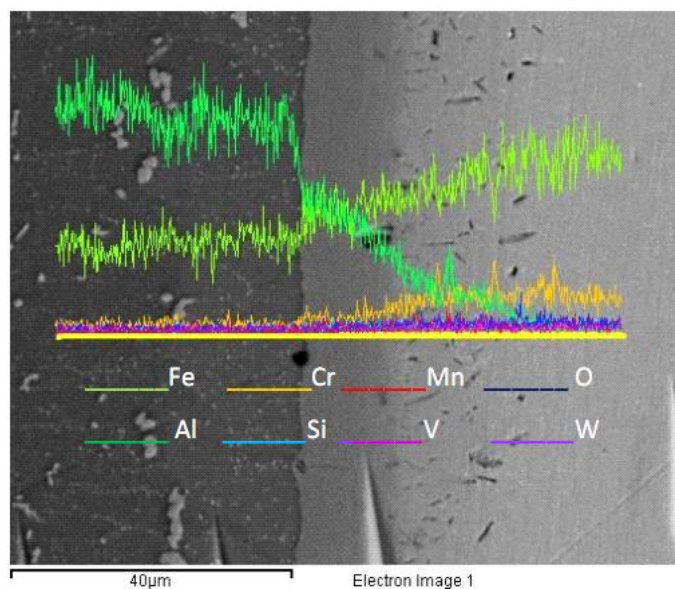


**Figure 6** EDX line scan analysis for sample F

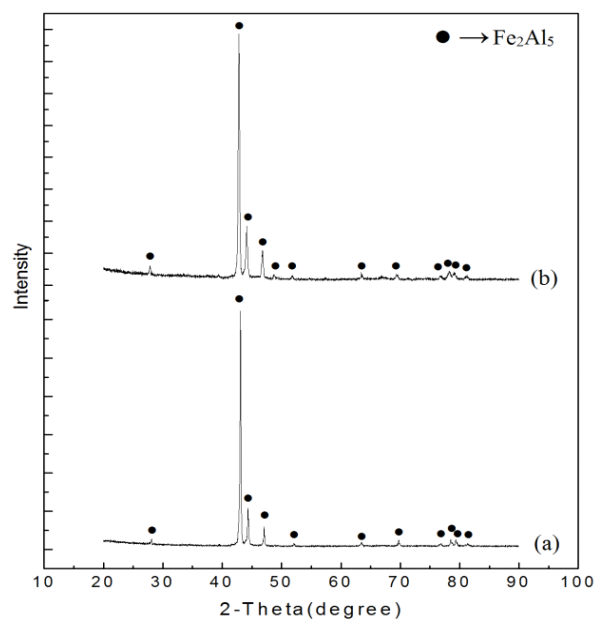


**Figure 7** XRD peaks for (a) sample A; and (b) sample D

### Scratch Adhesion test

**Figure 8** and **Figure 9** show scratch tests performed across the cross-section of the aluminized and heat-treated samples at 3 N and 5 N constant loads respectively. Very few cracks were observed at 3 N load as compared to 5 N load for all the samples. When a constant load of 3 N was applied, no cracks were formed in the inner diffusion layer (both intermediate zone and porous band) and very few cracks were observed in the outer diffusion layer for all the samples except that for sample F, where no crack was observed. It was found that the length of the cracks reduced with increase in the duration of heat treatment. It implies decrement in the brittle behaviour of the samples with increase in the duration of heat treatment. Thus on application of a constant load of 3 N, sample A was found to be most brittle whereas sample F was found to be most ductile.

When a constant load of 5 N was applied on the samples, multiple cracks were noted as the indenter moved from the substrate side to the coating zone. No cracks were formed in the inner diffusion layer (both intermediate zone and porous band) whereas multiple cracks were formed in the outer diffusion layer. Few cracks in the inner diffusion layer

depicted in Figure 9 are actually originating in the outer diffusion layer, some portion of which gets extended in the inner diffusion layer. From Figure 9 it was found that the number of cracks and length of cracks decreased with increase in the duration of heat treatment. At 5 N load, outer diffusion layer of sample F demonstrated very few cracks indicating sample F to be most ductile. This indicated that sample F exhibits better performance than other samples.

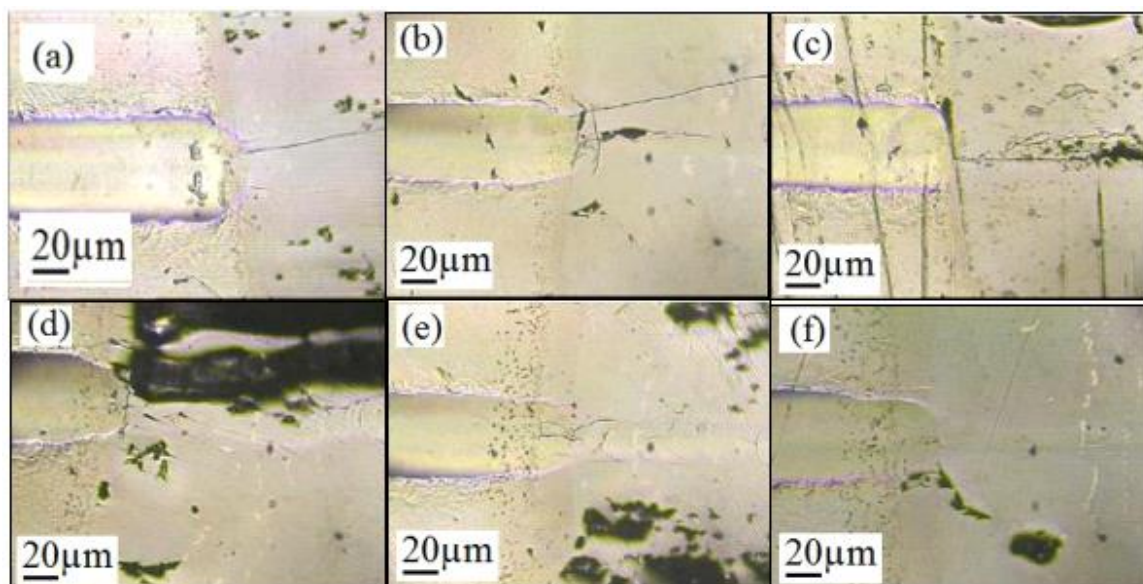


**Figure 8** Scratch results at 3N load across the cross-section of RAFM steel (a) sample A; (b) sample B; (c) sample C; (d) sample D; (e) sample E; and (f) sample F

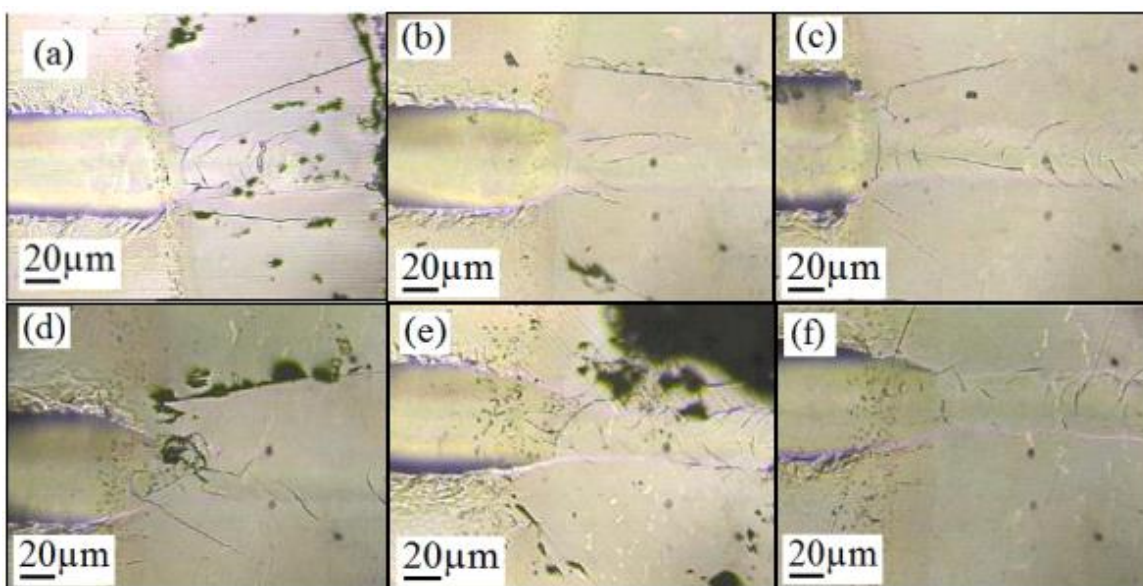


**Figure 9** Scratch results at 5N load across the cross-section of RAFM steel (a) sample A; (b) sample B; (c) sample C; (d) sample D; (e) sample E; and (f) sample F

There is no reported work in the open literature on scratch tests of the aluminized coatings on RAFMS. However, the scratch results have been discussed previously by one of the present authors in his previous work on aluminized coating on Modified Grade 91 Steel [17]. RAFMS structure in the ITER-TBM would see the flow of Pb-Li liquid melt at conditions specified in references [1, 2]. However, ductile phases FeAl and  $\alpha$ -Fe(Al) phases are the preferred phases after the heat treatment in the aluminized RAFMS. These phases could give the adhesion strength as high as

30N during scratch tests [17]. In the present work, we can see that the intermediate zone consisting of FeAl phase and the porous band consisting of FeAl+Fe<sub>3</sub>Al+ $\alpha$ -Fe(Al) phases did not show cracks up to the test loads of 5N. However, scratch loads could not be increased further here due to the presence of thick outer diffusion layer consisting of brittle Fe<sub>2</sub>Al<sub>5</sub> phase, which showed cracks at 5N load. Further work is required to be carried out to decrease the brittle phase and increase the ductile phases.

Penetration depth, friction force and AE curves were recorded online during scratch test for all the samples. A few representative graphs are shown. All the samples showed two distinct values of friction force – a higher value on the substrate side and a lower value on the coating side. Friction force on the substrate side varied between 0.3-0.4 N at 3 N applied load and 0.7-0.9 N at 5 N applied load. On the coating side, the friction force varied between 0.1-0.2 N at 3 N applied load and 0.2-0.4 N at 5 N applied load. **Figure 10** shows the comparative graphs of friction force for samples C and E at 3 N and 5 N loads. For sample C at 3 N applied load, friction force varied around 0.4 N on the substrate side and around 0.2 N on the coating side. When the load was increased to 5 N, friction force increased to 0.85 N (average value) on the substrate side and 0.4 N (average value) on the coating side. For sample E, friction force decreased from 0.7 N to 0.3 N (average value) on the substrate side when the load was decreased from 5 N to 3 N, whereas on the coating side the value was <0.2 N at both the loads. As the duration of heat treatment was increased, friction force continuously decreased with diminutive value on the coating side at the same applied load. Penetration depth was found to increase with the increase in load. **Figure 11** shows the AE graphs for aluminized and heat treated samples obtained during scratch tests. On the substrate side a flat lower value was obtained while on the coating side, sharp increase in the AE value with broad spectrum was obtained for all the samples. This indicates acoustic energy released on the coating side due to the cracks or other phenomena occurring.

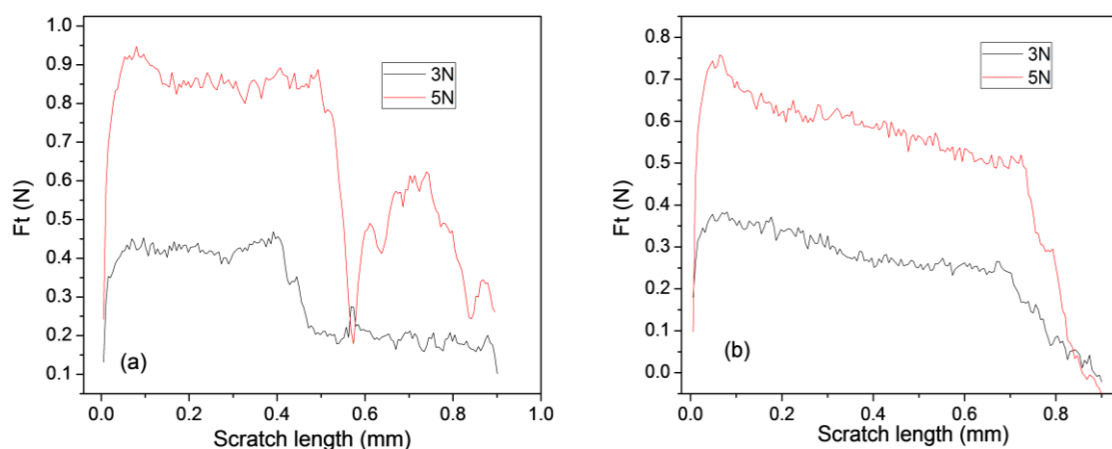


**Figure 10** Friction force graphs at 3 and 5 N loads for (a) sample C; and (b) sample E

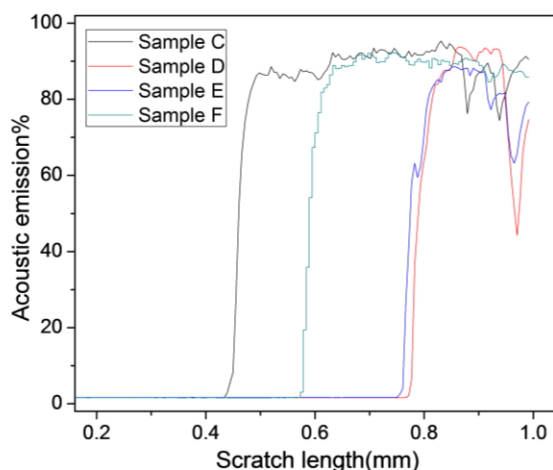


**Figure 11** Acoustic emission graphs obtained during scratch tests at 3 N load



## Conclusions

Hot dip aluminizing was carried out on RAFMS samples at 750 °C. Aluminized samples were heat treated at 750 °C for 5, 10, 15, 25, 50 and 75 h. Air cooling was employed after soaking. Effect of duration during heat treatment was studied on the morphology, elemental composition, phases, hardness and adhesion of the coatings. Following conclusions were drawn:

- Varying the duration of heat treatment affects the thickness and chemical composition of the diffusion layers.
- All the samples showed a wide outer diffusion layer and a thin inner diffusion layer. The inner diffusion layer consisted of two sub-zones; an intermediate zone and a porous band. There was little variation in the thickness of outer diffusion layer, while inner diffusion layer thickness increased with increase in the duration of heat treatment.
- Hardness of the outer diffusion layer was more as compared to the hardness of inner diffusion layer. This was due to the presence of Fe<sub>2</sub>Al<sub>5</sub> phase in the outer diffusion layer and presence of FeAl, α-Fe(Al) and FeAl<sub>3</sub> phases in the inner diffusion layer.
- EDX analysis showed Fe:Al ratio in the outer diffusion layer was ~1:2.5 (Fe<sub>2</sub>Al<sub>5</sub> phase), in the intermediate zone the ratio was ~1:1 (FeAl phase) and in the porous band it varied from 1:0.43 to 1:0.9 (FeAl+Fe<sub>3</sub>Al+α-Fe(Al) phases). This showed increase in the amount of Fe rich phase with increase in the duration of heat treatment.
- XRD performed on the outer diffusion layer showed the presence of Fe<sub>2</sub>Al<sub>5</sub> phase.
- During scratch tests, inner diffusion layer of all the samples showed no cracks upto 5N load. Outer diffusion layer showed no cracks at 3N load and nominal cracks at 5N load for sample heat treated for 75 h as compared to other samples which showed more cracks. All the samples showed two distinct values of friction force – a higher value on the substrate side and a lower value on the coating side.
- Further study is required to design the heat treatment which suppresses the formation of porous band, increase the amount of tough phases and decrease the brittle phases.

## References

- [1] E Rajendra Kumar, C Danani, I Sandeep, ChChakrapani, N Ravi Pragash, V Chaudhari, C Rotti, PM Raole, J Alphonsa, SP Deshpande, *Fusion Engineering and Design*, 2008, 83, 1169-1172.
- [2] P Chaudhuri, E Rajendra Kumar, A Sircar, S Ranjithkumar, V Chaudhari, C Danani, B Yadav, R Bhattacharyay, V Mehta, R Patel, KN Vyas, RK Singh, M Sarkar, R Srivastava, S Mohan, K Bhanja, AK Suri, *Fusion Engineering and Design*, 2012, 87, 1009-1013.
- [3] KS Forcey, APerujo, F Reiter, PL Lolli-Ceroni, *Journal of Nuclear Materials*, 1993, 200, 417-420.
- [4] A Perujo, KS Forcey, T Sample, *Journal of Nuclear Materials*, 1993, 207, 83.
- [5] L Giancarli, L Baraer, B Bielak, M Eid, M Futterer, C Nardi, *Fusion Technology*, 1994, 28, 1079-1085.
- [6] L Giancarli, JP Bonal, A Caso, G Le Marois, NB Morley, JF Salavy, *Fusion Engineering and Design*, 1998, 41, 165-171.
- [7] Z Zhu, M Zhang, S Gao, Y Song, C Li, L Peng, Z Guo, Y Wang, S Liu, M Kong, QHuang, FDS Team, *Fusion Engineering and Design*, 2009, 84, 5-8.
- [8] DL Smith, JH Park, I Lyublinski, V Evtikhin, A Perujo, H Glassbrenner, T Terai, S Zinkle, *Fusion Engineering and Design*, 2002, 61, 629-641.
- [9] YY Liu, DL Smith, *Journal of Nuclear Materials*, 1986, 141, 38-43.
- [10] Dai-Kai Sze, Michael C Billone, Thanh Q. Hua, Mark Tillack, FarrokhNajmabadi, Xueren Wang, *Fusion Engineering and Design*, 1998, 41, 371-376.
- [11] IR Kirillov, IV Danilov, SI Sidorenkov, Yu S Strebkov, RF Mattas, Y Gohar, TQ Hua, DL Smith., *Fusion Engineering and Design*, 1998, 39, 669-674.
- [12] Y Gohar, S Majumdar, D Smith, *Fusion Engineering and Design*, 2000, 49, 551-558.
- [13] MS. Tillack, ARIES Team, *Fusion Engineering and Design*, 1998, 41, 491-499.
- [14] J Konys, W Krauss, N Holstein, *Fusion Engineering and Design*, 2010, 85, 2141-2145.
- [15] H Glasbrenner, J Konys, *Fusion Engineering and Design*, 2001, 58, 725-729.
- [16] J Konys, W Krauss, Z Voss, O Wedemeyer, *Journal of Nuclear Materials*, 2007, 367, 1144-1149.

- [17] K Singh, AFernandes, B Paula, MR. Gonal, G Abraham, N Krishnamurthy, *Fusion Engineering and Design*, 2014, 89, 2534-2544.
- [18] S Han, H Li, S Wang, Li Jiang, Xi Liu, *International Journal of Hydrogen Energy*, 2010, 35, 2689-2693.
- [19] Fu-cheng YIN, Man-xiu ZHAO, Yong-xiong LIU, Wei HAN, Zhi LI. *Transactions of Nonferrous Metals Society of China*, 2013, 23, 556-561.
- [20] S Raju, B Jeya Ganesh, Arun Kumar Rai, R Mythili, S Saroja, E Mohandas, MVijayalakshmi, KBS Rao, Baldev Raj, *Journal of Nuclear Materials*, 2009, 389, 385-393.
- [21] H Glasbrenner, J Konys, *Fusion Engineering and Design*, 2001, 58, 725-729.
- [22] H Glasbrenner, O Wedemeyer, *Journal of Nuclear Materials*, 1998, 257, 274-281.
- [23] K Bouché, F Barbier, ACoulet, *Materials Science and Engineering*, 1998, 249, 167-175.
- [24] Fu-cheng YIN, Man-xiu ZHAO, Yong-xiong LIU, Wei HAN, Zhi LI, *Transactions of Nonferrous Metals Society of China*, 2013, 23, 556-561.
- [25] Li Yajiang, W. Juan, Z. Yonglan, X. Holly, *Bulletin of Materials Science*, 2002, 25, 635-639.
- [26] E Serra, H Glasbrenner, APerujo, *Fusion Engineering and Design*, 1998, 41, 149-155.
- [27] Y-J Li, J Wang, X Holly, *Materials Science and Technology*, 2003, 19, 657-660.

© 2015, by the Authors. The articles published from this journal are distributed to the public under “**Creative Commons Attribution License**” (<http://creativecommons.org/licenses/by/3.0/>). Therefore, upon proper citation of the original work, all the articles can be used without any restriction or can be distributed in any medium in any form.

#### Publication History

Received 10<sup>th</sup> July 2015  
Revised 18<sup>th</sup> July 2015  
Accepted 12<sup>th</sup> Aug 2015  
Online 30<sup>th</sup> Aug 2015